Polymer Bulletin (2024) 81:4819–4849
https://doi.org/10.1007/s00289-023-04915-1

ORIGINAL PAPER

Efficacy of co-loading Ag nanoparticles and metronidazole in PEG–gelatin-based sponges for the treatment of chronic wounds

Sibusiso Alven[1] · S. A. Adeyemi[2] · P. Ubanako[2] · D. T. Ndinteh[3] · Y. E. Choonara[2] · B. A. Aderibigbe[1]

Received: 30 December 2022 / Revised: 3 July 2023 / Accepted: 17 July 2023 /
Published online: 7 August 2023

Abstract

Polymer-based sponges loaded with antibacterial agents are potential wound dressings ideal for treating bacteria-infected wounds. Gelatin/poly (ethylene glycol) (PEG) sponge-based wound dressings loaded with metronidazole and Ag nanoparticles with different degrees of cross-linking were prepared, and their capability to treat infected wounds in vitro was evaluated. The degree of cross-linking of the sponges varied, and the porosity of the sponges was in the range of 15.64–91.10%. The amount of gelatin used to prepare the sponges influenced the porosity of the sponges. The sponges displayed an initial burst drug release of metronidazole followed by a sustained release profile. The sponges exhibited considerable antibacterial activity against Gram-positive and Gram-negative bacteria. The % cell viability of the sponges was in the range of 71.17–86.10%, indicating distinguished biocompatibility. The in vitro experiment showed that the sponge loaded with metronidazole, SAM2%, displayed a significant reduction of 66.68% in the scratch area compared to the sponge loaded with a combination of silver nanoparticles and metronidazole with a closure rate of 46.61% at 96 h. The promising features of the sponges indicate that they are potential wound dressings for treating infected wounds.

Keywords Infected wounds · Wound healing · Antibacterial activity · Biopolymers · Metronidazole · Metal-based nanoparticles

Introduction

Chronic wounds are life-threatening and are characterized by a delayed healing process, needing special clinical attention [1–3]. Examples of chronic wounds are ischemic, diabetic foot ulcers, and burns [4]. Microbial infection is the main cause

Extended author information available on the last page of the article

of retarded process of wound healing in most chronic wounds, causing the wound to remain in the inflammatory phase for a prolonged period [5–7]. Infections in patients with chronic wounds are the cause of extended hospital stays and amputations in severe cases [8]. The world health organization (WHO) reported that more than 2 million infections are caused by multi-drug resistant bacteria, with indirect and direct costs of treatment surpassing 55 billion dollars every year [9]. The currently used antimicrobial drugs suffer from antibacterial resistance that can subsequently result in increased morbidity caused by infected wounds globally [10, 11]. There is a pressing need for the development of effective wound dressings that possess potent antimicrobial activity. Wound dressings have been developed from different synthetic and biopolymers.

Wound dressings that are mostly fabricated from biopolymers (e.g., gelatin, alginate, cellulose, etc.) and synthetic polymers (e.g., polyvinylpyrrolidone (PVA), poly (lactic-co-glycolic acid) (PLGA), (polyglycolic acid (PGA), poly(ethylene glycol) (PEG), etc.) are employed to manage infected chronic wounds. In this study, gelatin was explored in combination with gelatin and PEG to prepare potential wound dressings for treating infected wounds. Gelatin is a solid, tasteless, and colorless biopolymer produced from the hydrolysis of collagen. It can be categorized based on its sources, such as fish, bovine, or porcine gelatin [12]. Fish gelatin used in this research study is made up of 85–92% protein, water, and mineral salt. Gelatin possesses promising biocompatibility and biodegradability and can be processed in any shape [13, 14]. PEG, on the other hand, is an inert, hydrophilic, non-immunogenic, compatible, and non-toxic synthetic polymer, making it appropriate for the design of wound dressings [15]. Furthermore, it is a water-swellable polymer with a high degree of elasticity, an excellent feature for tissue regeneration [16]. Some research studies have demonstrated that PEG-based wound dressings accelerate the wound healing process, the formation of granulation tissue, re-epithelialization, and neovascularization [17]. Due to the interesting properties of gelatin and PEG, these polymers were used for the formulation of sponge wound dressing scaffolds.

Sponges are flexible and soft wound dressing scaffolds that are characterized by interconnected microporous structures [18]. Their porous structures promote high water absorption, high swelling capacity, and hemostatic activity and also provide moisture for an accelerated process of wound healing and protection of the wound from bacterial invasion [19, 20]. In addition, sponges exhibit porosity in the range of 10–100 μm, a feature useful for the high rate of cell adhesion and proliferation during the wound healing process [21]. This research reports the preparation, characterization, and in vitro studies of gelatin–PEG-based hybrid sponges as promising wound dressings. The effect of the amount of gelatin and the % of cross-linking was evaluated on the porosity and biological activity of the sponges. Gelatin-based sponges have been tailored with varied degrees of cross-linking to control the drug release profile. The degree of cross-linking of the sponges has been widely reported to influence some of their features, such as porosity, biocompatibility, biodegradability, mechanical, and antibacterial properties [22–25]. However, the use of gelatin for the development of wound dressings is limited by its poor antibacterial activity.

In this study, the sponges were loaded with a combination of an antibiotic, metronidazole and metallic nanoparticles, Ag nanoparticles to promote synergistic

antibacterial activity. Research findings have demonstrated that the combination of metal-based nanoparticles with antibiotics enhances the efficacy of the antibiotic [26]. Metronidazole, a nitroimidazole derivative of antibiotics, is utilized for the treatment of several infections. It exhibits antibacterial activity against gram-positive *bacilli*, sporulated anaerobic *cocci*, and gram-negative anaerobic *bacilli*. However, its mode of action is not completely understood. It has been reported that metronidazole inhibits the synthesis of deoxyribose nucleic acid (DNA) and replication in bacteria, resulting in bacterial cell death [27–29]. In wound treatment, metronidazole is known as an effective therapeutic agent in controlling wound odor [30]. Metal-based nanostructures have also been widely investigated as antimicrobial agents, revealing their potential applications in the treatment of infected wounds [31, 32]. Ag nanoparticles are metal-based nanoparticles and are effective bioactive agents with good antimicrobial activities against a wide variety of microorganisms, such as bacteria, viruses, yeasts, and fungi [33]. The antimicrobial activity of Ag nanoparticles is due to their ability to destroy proteins of the bacterial cell membrane and interact with DNA [34–36]. Some preclinical studies have shown improved therapeutic outcomes of metal-based nanoparticles when combined with antibiotics in gelatin-based sponges for the treatment of infected wounds, resulting in excellent antibacterial effects and an accelerated rate of wound healing [37, 38]. Based on the promising features of gelatin-based sponges loaded with bioactive agents, this current study presents the efficacy of combining antibiotics and Ag nanoparticles in PEG–gelatin-based sponges and the effect of the content of gelatin in the sponges on the treatment of infected wounds.

Materials and methods

Solvents and reagents

Distilled water was utilized for the preparation of the wound dressing sponges. Gelatin, polyethylene glycol 4000 (PEG) ($M_n = 4000$ Da), metronidazole, silver nitrate ($AgNO_3$), trisodium citrate, and calcium chloride ($CaCl_2$) were purchased from (Merck Chemicals, South Africa). The reagents were utilized without additional purification.

Experimental

Preparation of Ag nanoparticles

The Ag nanoparticles were prepared using the Turkevich method [39, 40]. Briefly, silver nitrate ($AgNO_3$) solution (60 mL, 1 mM) was heated with stirring and covered with aluminum foil. Trisodium citrate solution (6 mL, 10 mM) was added dropwise with continuous stirring until a yellow–brown color was formed, confirming the formation of Ag nanoparticles. The solution was allowed to cool at room temperature and then, stored in the refrigerator until further use.

Preparation of the sponges

The sponges were prepared using a freeze-drying procedure [41–43]. Gelatin was dissolved in 20 mL of warm distilled water. PEG was dissolved separately in 20 mL of distilled water at room temperature. Both solutions were combined and stirred for 1 h. Metronidazole (80 mg) was added followed by the addition of 10 mL of Ag nanoparticle solution. The reaction was stirred for 1 h at room temperature followed by the addition of 2 or 5% $CaCl_2$ as a cross-linking agent. The solution was frozen at − 20 °C overnight and freeze-dried at − 60 °C for 24 h to afford the sponges. The prepared sponges were stored in a desiccator till further studies. The amount of polymers and bioactive agents used for the preparation of the sponges are presented in Table 1.

Characterization techniques

Freeze-drying

The sponges were freeze-dried after preparation on a Vir Tis benchtop K, Gardiner, New York.

Table 1 Composition of sponges

Sample name	Gelatin (mg)	PEG (mg)	Metronidazole	Ag nanoparticles	Cross-linking agent (%)
SA 1	200	200	80 mg	10 ml	5
SA 2	200	200	80 mg	10 ml	2
SA 3	300	200	80 mg	10 ml	5
SA 4	300	200	80 mg	10 ml	2
SA 5	400	200	80 mg	10 ml	5
SA 6	400	200	80 mg	10 ml	2
SA 6	500	200	80 mg	10 ml	5
SA 8	500	200	80 mg	10 ml	2
SA 9	600	200	80 mg	10 ml	5
SA 10	600	200	80 mg	10 ml	2
SA 11	700	200	80 mg	10 ml	5
SA 12	700	200	80 mg	10 ml	2
SAA2%	200	200	–	10 ml	2
SAA5%	200	200	–	10 ml	5
SAM2%	200	200	80 mg	–	2
SAB2%	200	200	–	–	5
SAB5%	200	200	–	–	5

UV-vis spectroscopy

UV-vis analysis was performed to confirm the formation of the Ag nanoparticles by evaluating the absorption peak using Lambda 365 UV-vis spectrometer, PerkinElmer, Korea.

Fourier transform infrared spectroscopy (FTIR)

Attenuated Total Reflection–Fourier Transform Infrared (ATR–FTIR) spectroscopy was performed on the sponges to determine the presence of functional groups using PerkinElmer Spectrum 100 FTIR Spectrometer, USA. The spectra were carried out in the range of 4000–500 cm^{-1}, running Omnic software for 64 scans and a resolution of 4 cm^{-1}.

Scanning electron microscopy (SEM)

The sponges were sputtered with gold particles before SEM analysis. SEM analysis was carried out to evaluate the morphology of the sponges. This analysis was performed at an accelerating voltage of 15 kV on JEOL JSM-6390LV Scanning Electron Microscope, Japan.

Thermogravimetric analysis (TGA)

TGA was utilized to evaluate the moisture content and thermal stability of sponges. It was performed using TG-analyzer (TGA-4000, Rheometric Scientific, South Africa). The amount of sponges used was in the range of 5–14 mg and was loaded on the TGA analyzer. The profile of weight loss was recorded from 20 to 700 °C at a heating rate of 10 °C per minute with a constant nitrogen flow of 50 mL/ min.

X-ray diffraction analysis (XRD)

XRD was performed on the metronidazole and the sponges using PANalyticalX'Pert PRO (USA) at 45 kV and 40 mA. The analysis was performed to determine the amorphous nature of the sponges and to confirm the successful loading of the bioactive agents into the sponges. The samples were filled into a hole between 1 and 2 mm in diameter in a piece of metal ~ 1.5 mm thick. The metal piece was then fixed on a specimen container so that the X-ray beam could pass through. Data were collected within the range of $2\Theta = 10–80$, scanning at 1.5 min^{-1} with a time-constant filter of 0.38 s per step and 6.0 mm slit width.

Porosity

The porosity study was performed to determine the degree of porosity of the sponges by liquid displacement procedure using ethanol as the displacement liquid

due to its capability to readily penetrate through the pores of the wound dressing scaffolds without causing shrinking [22, 44, 45]. The freeze-dried sponges (10 mg) were placed in 2 mL of ethanol and weighed after an hour.

The sponge porosity was calculated using the following Eq. 1:

$$\text{Porosity} = \frac{W_2 - W_1}{p \cdot V} \tag{1}$$

where W_2 is the mass of sponges after immersion in ethanol $W1$ is the mass of sponges before immersion in ethanol. V is the volume of the sponges. p is the density of ethanol.

In vitro drug release studies

The in vitro drug release studies were performed on the sponges according to the method by Wen et al. [42] and Tawfeek et al. [46]. 20 mg of each prepared sponge was dissolved in 3 mL of phosphate buffer saline (PBS) (pH 7.4) simulating physiological pH. The solution was poured into the dialysis membrane and incubated in 40 mL of PBS at 37 °C with slow shaking. The release media was emptied and replaced with a fresh buffer solution at 1 h intervals for 8 h followed by 24 and 48 h to determine the concentration of the drug released from the sponges using a UV-vis spectrometer. The UV-vis experiments of the released bioactive agents from the sponges were performed at the wavelengths of 320 nm and 430 nm, for metronidazole and Ag nanoparticles, respectively. The obtained data were expressed as % cumulative drug release. The concentration of metronidazole and Ag nanoparticles released from the sponges was investigated using a calibration curve. The measurements were performed in triplicate for each sponge. The percentage of drug release was calculated using Eq. 2:

$$\%\text{drug release} = \frac{\text{Amount drug released}}{\text{Amount drug} - \text{loaded}} \times 100\% \tag{2}$$

The selected drug release mathematical models that were used to determine the release mechanisms of the loaded bioactive agents from the sponges are Zero-order, Korsmeyer–Peppas, and Higuchi equations.

i. Zero-order release equation

The equation of the Zero-order release model is shown in Eq. 3:

$$Q = K \cdot t + Q_o \tag{3}$$

where Q is the amount of the bioactive agent dissolved in time t, Q_o is the initial amount of the bioactive agent loaded in the sponge, and K is the Zero-order release constant. This equation refers to a release profile of a bioactive agent that is independent of the amount of bioactive agent in the sponges at a constant rate. The data obtained from the in vitro drug release experiments were plotted as % cumulative drug release versus time.

ii. Korsmeyer–Peppas release equation

The equation of the Korsmeyer–Peppas release model is shown in Eq. 4:

$$Q = Mt/M\infty$$

$$Mt/M\infty = K \cdot t^{n} \tag{4}$$

where $Mt/M\infty$ is the amount of the released bioactive agent at time t. K and I are the release rate constant and release exponent, respectively. The n value is utilized to describe different release profiles of the delivery system This release model illustrates drug release from a polymeric system. Only the first 60% of drug release data can be fitted in the Korsmeyer–Peppas model to determine the drug release mechanism. To evaluate the release kinetics, the data obtained from the in vitro drug release experiments were plotted as log cumulative percentage drug release versus log time (Table 2).

iii Higuchi release equations

The equation of the Higuchi release model is shown in Eq. 5:

$$Q = K\sqrt{t} \tag{5}$$

where K is the Higuchi dissolution constant and Q is the amount of drug released in time t. This equation refers to a system where the drug release is via diffusion. This model is suitable for porous delivery systems. The data obtained were plotted as % cumulative drug release versus square root of time.

In vitro cytotoxicity evaluation

The in vitro cytotoxicity evaluation of the sponges was performed to evaluate their biocompatibility employing the 3-(4,5-dimethylthiazol-2-yl)-2,5-diphenyltetrazolium bromide (MTT) assay. The sponges were screened against HaCaT cells (immortalized human keratinocytes) which were cultured at a density of $5X10^4$ cells/mL in a 96-well plate at a volume of 90 µL/well. Twenty-four hours later, the cells were treated in triplicates with 10 µL of the sponge solution, making final concentrations of 100, 50, 25, and 12.2 µg/mL. Cells treated with 1X PBS (phosphate-buffered saline) and 10% DMSO served as the negative and positive controls, respectively. The 96-well plates were incubated for 48 h, after which MTT

Table 2 The diffusion coefficient (n) is used to determine the mechanism of release

Coefficient of diffusion value	Mechanism of release
$n < 0.5$	Quasi-Fickian Diffusion
$n = 0.5$	Fickian Diffusion
$0.5 < n < 1.0$	Anomalous (non-Fickian)
$n = 1.0$	Non-Fickian case II. It means a zero-order release profile
$n > 1$	Non-Fickian super case II

reagent was added. The plates were incubated for 4 h, solubilized overnight using the solubilization reagent, and the absorbance values were measured at 570 nm. The experiments were run in triplicate. The cytotoxicity results of the wound dressings were analyzed by calculating the percentage cell viability of each sponge against the untreated cells using Eq. (6) shown below:

$$\%\text{cell viability} = \frac{\text{OD}_s - \text{OD}_\text{b}}{\text{OD}_\text{u} - \text{OD}_\text{b}} \times 100\% \tag{6}$$

where OD_S is the absorbance of the compound and OD_b is the absorbance of the blank. OD_u is the absorbance of the untreated compound.

In vitro antibacterial studies

The minimum inhibitory concentration (MIC) of the sponges was performed according to the protocol reported by Fonkui et al. [47]. Each compound was dissolved in distilled water to a stock concentration of 1 mg/mL. These solutions were then serially diluted (6 times) in 100 uL of nutrient broth in 96 well plates to the anticipated concentrations (500, 250, 125, 62.5, 31.25, and 15.625 µg/mL). Then after, 100 µL of each of these solutions was located in duplicate and incubated with 100 µL of overnight bacterial culture in a 0.5 Mc Farland in nutrient broth. Ampicillin, nalidixic acid, and streptomycin were utilized as positive controls, and the negative control was formulated to contain 50% of nutrient broth in DMSO.

In vitro scratch wound healing assay

In vitro scratch wound healing is an affordable study utilized to analyze fibroblast cell migration in two dimensions to induce wound healing. In vitro wound healing assay was evaluated based on a procedure adapted from Felice et al. [48], Suarez-Arnedo et al. [49], Cheng et al. [50], and Ranzato et al. [51]. Immortalized human keratinocyte (HaCaT) cells were cultured in a humidified incubator at 37 °C and 5% CO_2 to 90% confluency in Dulbecco's Modified Eagle's Medium (DMEM) containing 10% (v/v) fetal bovine serum (FBS) and 1% (v/v) penicillin–streptomycin (Penstrep) antibiotics. The cells were then trypsinized, and viable cells were quantified employing the trypan blue dye elimination method. The cell density was adjusted to 2.5×10^5 cells/mL, and the cells were incubated in 6-well plates until cell monolayers were formed (48 h later). Single scratch wounds per well were generated utilizing a 200 µL micropipette tip. The cells were then washed once per well with 2 mL of 1X phosphate-buffered saline (1X PBS) to remove dislodged cells. Serum-poor DMEM medium (containing 1% FBS) was added to the wells (1800 µL per well), and cells were treated with 200 µL of the solution of the wound dressings of various concentrations that showed the highest viability on the MTT assay screen.

Untreated cells seeded in Dulbecco's Modified Eagle's Medium (DMEM) containing 10% FBS were used as positive control while those cultured in 1% Fetal Bovine Serum (FBS) in DMEM were employed as the negative control. The images were captured in duplicates at 0, 24, 48, 72, and 96 h using the 4X objective and

phase-contrast feature of an inverted light microscope (Olympus CKX53, Olympus, Tokyo, Japan). Cell migration was quantified using ImageJ image processing software.

Statistical analysis

All data obtained for the in vitro studies were analyzed using Student's unpaired *t*-test on GraphPad Prism version 9 (GraphPad Software, Inc., San Diego, CA, USA). All data are expressed as mean ± standard deviation in triplicate ($n = 3$), and a *p*-value of < 0.05 was considered significant.

Results and discussion

UV-vis

UV-vis spectroscopy was employed to confirm the successful formation of Ag nanoparticles by analyzing the absorbance data. The UV-vis spectrum of Ag nanoparticles displayed a wide visible absorbance band at 426 nm (Supplementary Fig. 1). Alim-Al-Razy et al. prepared Ag nanoparticles utilizing the Turkevich procedure. The UV-vis results of Ag nanoparticles were reported to exhibit characteristic peaks between 417 and 444 nm, depending on the concentration of $AgNO_3$ [52]. The Ag nanoparticles synthesized by Singh et al. utilizing green synthesis reported an absorbance band at 427 nm, confirming the result reported in this study [53]. Anandalakshmi also reported Ag nanoparticles with an absorption peak at 430 nm [54].

FTIR

The FTIR spectra of gelatin–PEG hybrid sponges loaded with metronidazole and Ag nanoparticles are shown in Fig. 1a–c, including the blank sponge. The FTIR spectra of hybrid sponges displayed similar characteristic absorption peaks due to their composition. The characteristic peaks were visible between 1637 and 1628 cm^{-1} (amide I), 1545 or 1536 cm^{-1} (amide II), and 1261–1243 cm^{-1} (amide III), due to the C=O stretching vibrations of amides for gelatin. Furthermore, the C= O stretching vibrations of amide III of gelatin were visible at 1261–1243 cm^{-1} and overlapped with C–O stretching vibrations that confirmed the presence of PEG in sponges. Several researchers reported similar FTIR results for gelatin-based scaffolds for wound dressing applications [55–58].

The C=N stretching vibration at 1545 or 1536 cm^{-1} (overlapped with amide II of gelatin), N=O asymmetric stretching at 1472–1436 cm^{-1} (overlapped with amide III of gelatin), C–C stretching at 1426 or 1416 cm^{-1}, CH_3 bending vibration at 1371–1343 cm^{-1}, C–N stretching vibration at 1078–1059 cm^{-1}, and =C–H bending at 785–785 cm^{-1}, confirmed the functional groups of metronidazole, revealing its successful loading in the sponges (SA1–SA12, and SAM2%). Furthermore, the peaks between 3351 and 3218 cm^{-1} denote the O–H stretching vibrations of

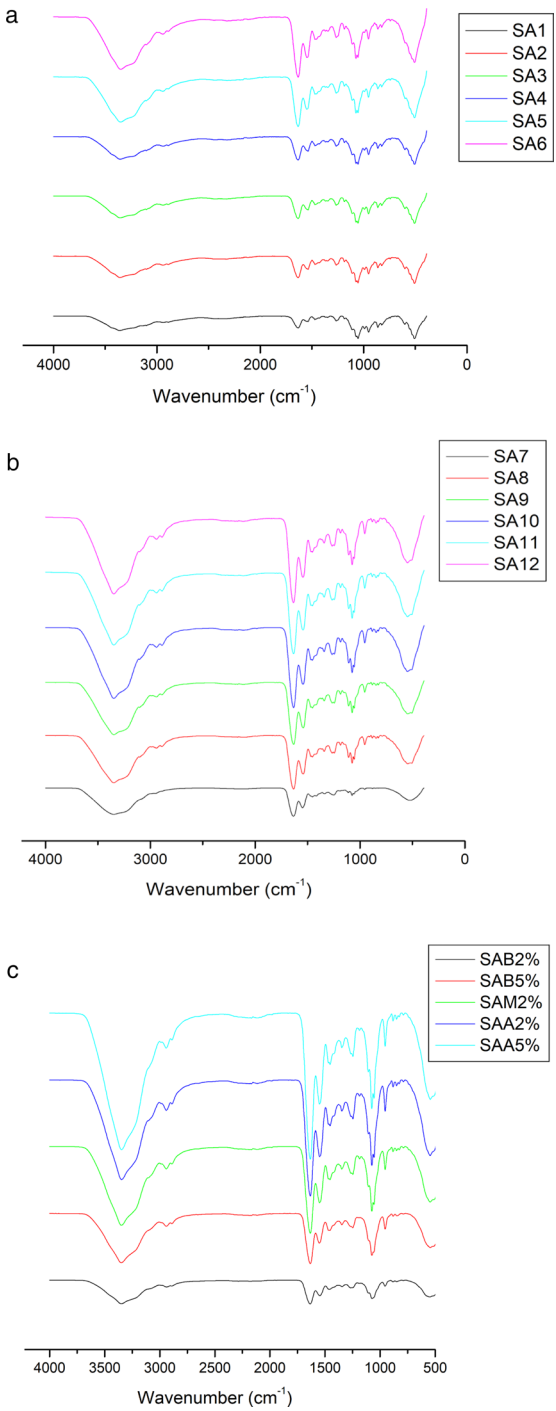

Fig. 1 **a** FTIR spectra of sponges SA1–6. **b** FTIR spectra of sponges SA7–12 **c** FTIR spectra of SAB2%, SAB5%, SAM2%, SAA2%, and SAA5%

metronidazole. These results are similar to those reported by Trivedi et al. for metronidazole [59]. The CH_3 bending at 1371–1344 cm^{-1} is ascribed to the methyl group of metronidazole and gelatin. Furthermore, the FTIR spectra of sponges containing Ag nanoparticles (SA1–SA12, SAA2%, and SAA5%) showed peaks in the range of 3351–3218 cm^{-1} for O–H stretching vibrations (overlapping with the O–H stretching vibration of metronidazole), 1545 or 1536 cm^{-1} signifying N–H bending vibration of primary amines overlapped with C=N stretching, 1078–1059 cm^{-1} (stretching vibrations of all amines), and the peaks between 958 cm^{-1} and 821 cm^{-1} (C–H bending vibrations out of plane). Arif et al. reported similar results for FTIR spectra of Ag nanoparticles [60]. The peak at 556 cm^{-1} represents the vibration frequency of the Ag–O bond [61]. The FTIR spectra of the drug-loaded sponges did not reveal any interaction of the therapeutic agents with the polymer matrix.

SEM/EDX

The SEM images of gelatin/PEG hybrid sponges are shown in Fig. 2, displaying the surface morphology of the sponges. The SEM images of SA1, SA3, and SA5 exhibited a combination of plate-like structures and sphere-shaped morphology. The surface morphology of SA2, SA6, SA12, SAA2%, and SAB2% also displayed plate-like structures. The SEM images of SA4 and SA7 showed globular morphology with microporous structures. The surface morphology of SA10 exhibited swollen morphology. The SEM images of SA8, SA9, SA11, and SAM2% showed porous network structures. The SEM images of SAA5% and SAB5% demonstrated a combination of globular morphology with sphere-shaped morphology. Similar micrographs were reported by Wang et al. for ECM-loaded gelatin sponges. Their SEM images showed highly porous network structures [62]. Several researchers have reported similar porous morphology for gelatin-based sponges resulting from the high amount of gelatin in the prepared sponges [25, 63–66].

The concentration of $CaCl_2$ used for cross-linking did not yield any significant effect on the morphology of the sponges. Ngece et al. reported SEM results of biopolymer-based sponges cross-linked using $CaCl_2$, and the concentration of the cross-linker did not produce any significant effect on the SEM images of the sponges [67]. The porous structure of the wound dressing is important for improved gaseous permeation and is suitable to induce high cell proliferation and attachment, nutrient migration, and acceleration of wound healing. Furthermore, the porous morphology also influences the water adsorption capacity of the sponges [14].

The EDX analysis was used to determine the % of AgNPs in the gelatin/PEG sponges (SA1–SA12) and (SAA2% and SAA5%). The mass percentage of Ag in the sponges was in the range of 0.10–1.13%. The EDX results revealed the successful incorporation of AgNPs in the sponges (Table 3).

Thermogravimetric analysis of the sponges

The Thermogravimetric analysis (TGA) was performed to evaluate the moisture content of the gelatin/PEG sponges. Ideal moisture content is effective in providing

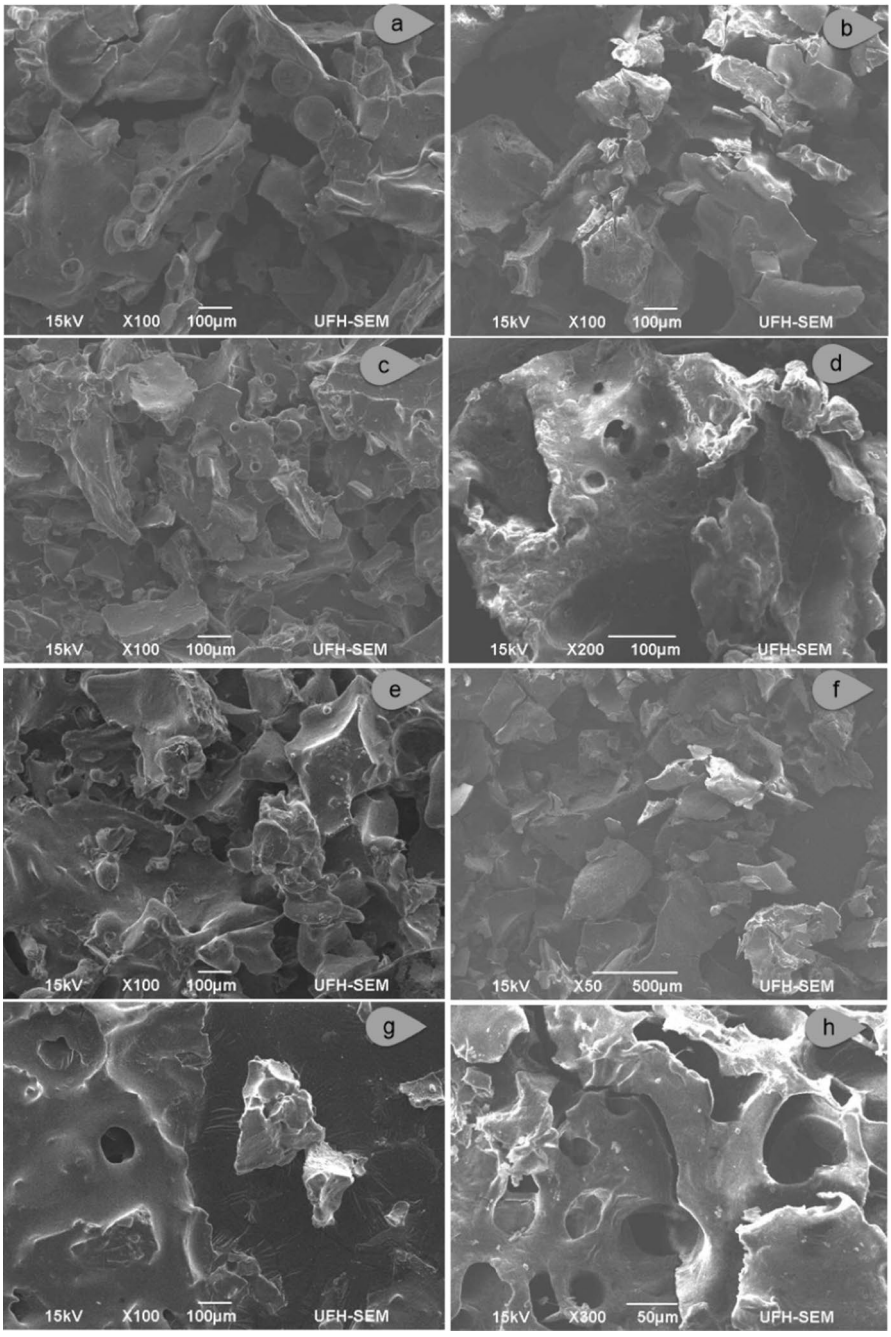

Fig. 2 SEM images of **a** SA1 **b** SA2 **c** SA3 **d** SA4. SEM images of **e** SA5 **f** SA6 **g** SA7 **h** SA8. SEM images of **i** SA9 **j** SA10 **k** SA11 **l** SA12 **m** SAA2% **n** SAA5% **o** SAB2% **p** SAB5 **q** SEM image of SAM2%

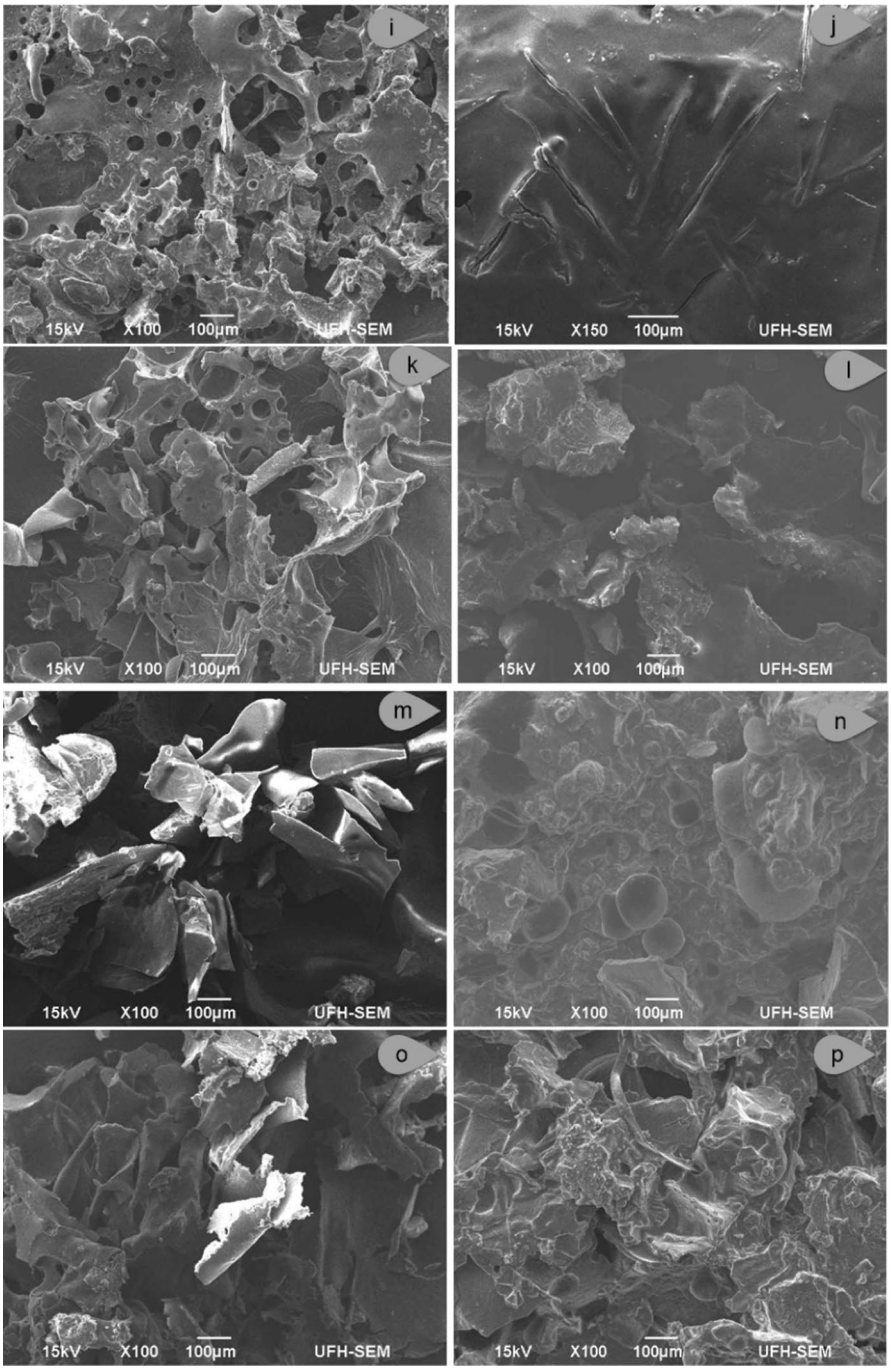

Fig. 2 (continued)

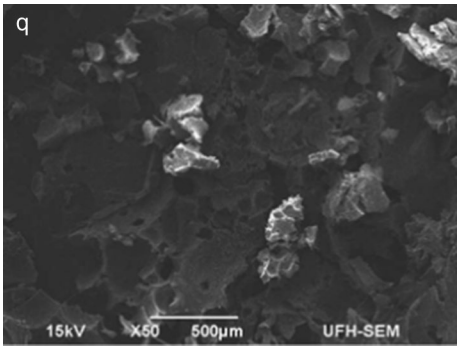

Fig. 2 (continued)

Table 3 The % of Ag in the prepared sponges

Sponges	Silver (Ag) (%)
SA1	0.52
SA2	–
SA3	–
SA4	0.48
SA5	0.92
SA6	0.20
SA7	0.26
SA8	0.85
SA9	–
SA10	0.10
SA11	0.15
SA12	1.13
SAA2%	–
SAA5%	0.91

an appropriate environment for accelerated wound healing [68]. The TGA thermographs of the sponges are shown in (Supplementary Fig. 2a–q). Sponges SA1, SA2, SA4, SA6, and SA8 showed four phases of weight loss of 12.96–22.76% at 32–125 °C, 9.07–18% at 106–258 °C, 20.10–37.68% at 243–448 °C, and 2.55–26.70% at 250–585 °C. Sponges SA3, SA5, SA7, SA9, SA10, SA11, and SA12 exhibited three distinct phases of weight loss of 14.70–28.81% at 28–224 °C, 28.38–44.19% at 126–432 °C, and 11.36–26.61% at 399–610 °C. Lastly, the sponges SAA2%, SAA5%, SAB2%, SAB5%, and SAM2% also displayed three significant stages of weight loss of 19.51–48.75 at 28–156 °C, 13–38.74% at 135–429, and 7.62–20.92% at 370–568 °C.

The first phase of weight loss of the gelatin/PEG sponges was due to the presence of moisture. Most of the sponges exhibited ideal moisture content that ranged between 12.96 and 27.28%, except SAA5% (40.65%) and SAB5% (48.75%), indicating their capability to offer a moist environment, a crucial feature for accelerated

Table 4 The moisture content of the sponges evaluated via TGA analysis and porosity

Sponges	Moisture content (%)	Porosity
SA1	22.76	21.59
SA2	14.78	81.84
SA3	27.28	42.85
SA4	13.60	76.70
SA5	25.75	71.76
SA6	13.65	77.99
SA7	28.81	43.44
SA8	12.96	64.60
SA9	18.89	39.71
SA10	15.70	89.81
SA11	14.70	78.71
SA12	19.21	77.39
SAA2%	23.71	91.10
SAA5%	40.65	15.64
SAB2%	19.51	68.00
SAB5%	48.75	22.56
SAM2%	25.55	81.30

wound healing. The moisture contents of the sponges are summarized in Table 4. The moisture content of the sponges was observed at a temperature that ranged between 28 and 224 °C. The final two phases of weight loss are attributed to the degradation of the sponges. The pattern of weight loss of the sponges was similar to gelatin-chitosan hybrid sponges fabricated by Lu et al. The TGA analysis of gelatin-based hybrid sponges exhibited three stages of weight; the first stage of weight loss at a temperature between 40 and 217 °C is attributed to the moisture content of the sponges [69]. Wen et al. prepared gelatin/sodium alginate hybrid sponges encapsulated with tetracycline hydrochloride to treat bacteria-infected injuries. The TGA thermographs showed the first phase of weight loss below 120 °C, due to the evaporation of moisture and the weight loss that occurred at the temperature between 180 and 370 °C was due to the degradation of the sponges [42]. Naghshineh et al. reported a first stage of weight loss at the temperature range of 170–300 °C for curcumin-loaded gelatin-based sponges which were also attributed to the moisture content of the sponges. The second and third phases were attributed to the release of volatile compounds, depolymerization of the polymer chain in sponges, degradation, etc. [63].

XRD analysis of the sponges

The XRD spectrum of metronidazole revealed significant crystalline characteristic peaks at $2\Theta = 12.50$, 13.90, 21.50, 24.90, 29.50, and 33.95 (Supp 3a). The XRD spectra of gelatin/PEG sponges showed broad peaks, demonstrating the amorphous nature of the sponges (Supp 3b–k). Some of the characteristic crystalline peaks of

metronidazole were not significant in the XRD graphs of the sponges. However, a distinctive peak was visible in all the sponges at $2\Theta = 12.50$, revealing the successful encapsulation of metronidazole in the sponges. Some researchers that prepared drug-loaded gelatin-based hybrid scaffolds for wound treatment reported the amorphous nature of the sponges [43, 70].

Porosity evaluation of the sponges

The % porosity of the gelatin-based hybrid sponges is shown in Table 4. The porosity of the hybrid sponges ranged between 15.64 and 91.10%. The increasing amount of gelatin utilized for the formulation of the hybrid sponges enhanced the % porosity of most of the hybrid sponges. In the case of sponges prepared using the same amount of gelatin, the sponges cross-linked with 2% $CaCl_2$ led to higher porosity than the sponges cross-linked with 5% $CaCl_2$, suggesting that the percentage of cross-linking agent affected the porosity of wound dressing. Sponge SAA2% displayed the highest porosity and was cross-linked with 2% $CaCl_2$ when compared to all the sponges, and it was loaded with only Ag nanoparticles. The sponge, SAA5%, displayed the lowest porosity and was cross-linked with 5% $CaCl_2$. These results demonstrate that the percentage of the cross-linking agents influenced the porosity of the sponges. Furthermore, the high % porosity of the sponges demonstrates that gelatin, a biopolymer plays a crucial role in enhancing the porosity of the wound dressings.

Ngece et al. formulated sponges from sodium alginate and gum acacia using $CaCl_2$ as a cross-linking agent. The porosity studies showed that the increase in the content of biopolymers used for the preparation of the sponges significantly improved the % porosity of the sponges. Furthermore, utilizing 2% of $CaCl_2$ for cross-linking of the sponges led to higher porosity than those cross-linked with 1% of $CaCl_2$ [67]. Most of the reported gelatin-based hybrid sponges exhibited good porosity, a feature useful for gaseous diffusion, migration of nutrients to the injury, permitting the exchange of substances between the cells of the skin, promoting the absorption of wound exudates, and stimulating high cell adhesion and proliferation useful for an acceleration of wound healing [71].

In vitro biodegradability studies

The in vitro biodegradability experiments were performed at pH 7.4 and 5.5, simulating physiological pH and a chronic wound environment, respectively. The biodegradability of the sponges was analyzed and confirmed by FTIR and SEM. The sponge selected for in vitro biodegradability are SA3, SA4, SA11, SA12, SAB2%, and SAB5% due to the different polymer compositions and percentages of the cross-linking agent. The FTIR spectra of the samples after biodegradation experiments at pH 7.4 are shown in Supp Fig. 4a–f.

The O–H stretching vibration at 3351–3218 cm^{-1} attributed to the O–H stretch of metronidazole was replaced by new and multiple peaks in all sponges after biodegradation. New peaks that appeared for SA3 were at 3377, 3130, and

3689 cm^{-1} after 1, 2, and 3 weeks of the biodegradation studies, respectively, revealing the degradable nature of the sponges. The O–H vibration peak on SA4 was not visible after one week, and two new peaks were formed at 3355 and 3376 cm^{-1} after 1 weeks of biodegradation studies. Also, the intensity of the O–H vibration peak of the SA4 was significantly reduced after three weeks. The O–H vibration peak of the SA11 was broad after three weeks of the biodegradation studies with the appearance of a new peak at 2429 cm^{-1}. The O–H peak of SA12 was much broader during weeks 1 and 2 of biodegradation, and a new vibration peak was formed at 2409 cm^{-1} after 3 weeks of biodegradation studies.

The O–H peak of SAB2% was broader after 1–2 weeks of biodegradation experiments, and a new peak was visible at 2434 cm^{-1} after 3 weeks of biodegradation. Furthermore, 2 new peaks were visible in the O–H range (3432 and 3376 cm^{-1}) during the third week of biodegradation studies. For SAB5%, the intensity of O–H vibration stretching was reduced during the 1 and 2 weeks of biodegradation, and 2 new peaks were visible at 3451 and 3377 cm^{-1}. A new broad peak was visible at 2397 cm^{-1} after 3 weeks of the biodegradation studies. The C=O vibration stretching at 1637–1628 cm^{-1} in all the gelatin-hybrid sponges loaded with metronidazole was less intense after degradation. The significant changes and the formation of new peaks after the 3 weeks of biodegradation studies confirmed that the sponges are biodegradable under physiological conditions. The SEM micrographs of the sponges after biodegradation at pH 7.4. are shown in Supp 5a–f. The SEM images showed rough surfaces for all the sponges after 1, 2, and 3 weeks of the biodegradation experiments. The significant change in the morphology of the sponges further confirmed the biodegradable nature of the sponges. The biodegradable nature of the sponges reveals their potential capability to induce skin regeneration.

The FTIR spectra of the sponges at the pH of 5.5 after biodegradation studies are shown in Supp 6a–f. The peaks between 3351 and 3218 cm^{-1} that denote the O–H stretching vibrations of metronidazole and Ag nanoparticles were absent in all the sponges after three weeks. The following peaks were reduced after three weeks in most of the sponges: the C=N stretching at 1545 or 1536 cm^{-1} (overlapped with amide II of gelatin), N=O asymmetric stretching at 1472–1436 cm^{-1} (overlapped with amide III of gelatin), CH_3 bending at 1371–1344 cm^{-1}, C–C stretching at 1426 or 1416 cm^{-1}, CH_3 bending vibration at 1371–1343 cm^{-1}, C–N stretching at 1078–1059 cm^{-1}, and =C–H bending at 785–785 cm^{-1}.

These changes confirmed that the sponges are degradable. The SEM micrographs of the sponges after biodegradation at pH 5.5 further confirmed the biodegradability of the sponges (Supp Fig. 7a–f). The morphology of SA3 changed from plate-shaped to rough surfaces at weeks 1 and 2, and a mixture of a sphere-shaped and rod-shaped morphology at week 3. SA4 SEM image displayed rod-shaped morphology at week 1, globular morphology at week 2, and block-shaped surface. SA11 displayed a rough surface in weeks 1 and 3. SA12 and SAB2% also exhibited a rough surface at weeks 1 and 3 of the biodegradation studies.

In vitro drug release

The in vitro drug release studies were performed on selected gelatin/PEG sponges (SA1, SA2, SA5, SA6, SA11, SA12, SAM2%, SAA2%, and SAA5%) loaded with bioactive agents (metronidazole and Ag nanoparticles). These studies were performed to evaluate the mode of drug release from the sponges at physiological conditions (pH 7.4, 37 °C). The graphs that display the release of metronidazole and Ag nanoparticles are shown in Supp Fig. 8a–i. The % cumulative drug release of metronidazole was 78.95%, 89.88%, 85.88%, 91.76%, 80.45%, 88.61%, and 86.41% for sponges SA1, SA2, SA5, SA6, SA11, SA12, and SAM2% for 24 h, respectively. The % cumulative drug release of metronidazole was 88.35%, 95.02%, 97.22%, 97.16%, 94.64%, 98.00%, and 98.64% from sponges SA1, SA2, SA5, SA6, SA11, SA12, and SAM2% for 48 h, respectively, indicating that almost all the loaded metronidazole was released from the sponges within 48 h.

An initial burst drug release was observed in the first hour from SA1, SA2, SA5, SA6, SA11, SA12, and SAM2%, respectively, resulting from the high drug solubility in aqueous systems, making it easily released through the porous scaffolds [72]. The burst drug release effect was followed by a sustained drug release profile for 48 h. The initial rapid release is advantageous for the management of wounds by offering immediate relief followed by sustained release to stimulate a continued healing process. The initial burst release followed by the sustained drug release significantly induced the fast killing of bacteria and the inhibition of persisting bacteria, as well as protecting the wound from further bacterial invasion [68]. Ye et al. reported the drug release profile of ampicillin from gelatin/bacterial cellulose hybrid sponges for antibacterial wound dressing application. An initial burst release of ampicillin in the first hour was attributed to the accumulation of the antibiotic on the surface of composite sponges, followed by a sustained drug release for 48 h [73].

The mathematical models utilized to evaluate the mechanisms of drug release from the sponges are Zero-order, Higuchi, and Korsmeyer–Peppas models. The values of R^2, n, and K of the drug release models of each sponge are summarized in Table 5. The correlation of coefficient (R^2) was used to evaluate the most appropriate model that describes the mechanism of drug release. The drug release mechanisms of the sponges (SA1, SA2, SA5, SA6, SA11, SA12, and SAM2%) for metronidazole fitted best into the Korsmeyer–Peppas model with R^2 ranging between 0.9189 and 0.9964, and n values of 0.9616, 0.8671, and 0.9118 for SA1, SA5, and SA12, respectively, representing a non-Fickian release mechanism (n values greater than 0.5). The n values of SA1, SA6, SA11, and SAM2% were 1.2383, 1.3771, 1.108, and 1.296, representing a non-Fickian super case II release mechanism (n values greater than 1).

The release of Ag nanoparticles from the sponges was sustained in the first hour with a % cumulative release of 10.46% for SA1, 10.20% for SA2, 8.69% for SA5, 10.75% for SA6, 15.56% for SA11, 10.34% for SA12, 13.62% for SAA2%, and 15.77% for SAA5%. The sustained drug release profile protects the wound from bacterial invasion and inhibits bacteria invasion during the wound healing process. The gelatin hybrid sponges exhibited slow and sustained drug release of Ag nanoparticles for 48 h with % cumulative drug release of 94.09%, 95.13%, 93.85%, 96.69%,

Table 5 The drug release analysis constants of sponges for the Zero-order, Higuchi, and Korsmeyer–Peppas

Sponge	Loaded drug	Zero-order model		Higuchi model		Korsmeyer–Peppas model		
		K	r^2	K	r^2	K	n	r^2
SA1	Metronidazole	0.067	0.9012	0.719	0.7072	0.2475	1.2383	0.9766
	Ag nanoparticles	0.1277	0.9981	3.8366	0.9881	0.8767	0.5405	0.9992
SA2	Metronidazole	0.0953	0.8668	2.9981	0.9407	0.3763	0.9616	0.9543
	Ag nanoparticles	0.1264	0.9884	3.7521	0.9555	0.8535	0.5213	0.9861
SA5	Metronidazole	0.098	0.9704	2.9906	0.9909	0.3783	0.8671	0.9891
	Ag nanoparticles	0.1265	0.9986	3.7744	0.9745	0.9345	0.7383	0.9964
SA6	Metronidazole	0.059	0.7429	0.668	0.6668	0.2198	1.3771	0.9189
	Ag nanoparticles	0.1083	0.9168	3.29240	0.9894	0.8025	0.3526	0.9750
SA11	Metronidazole	0.0958	0.9741	2.9231	0.9944	0.2743	1.108	0.9622
	Ag nanoparticles	0.0906	0.9842	2.7186	0.9726	0.5638	0.1896	0.9760
SA12	Metronidazole	0.096	0.9044	1.086	0.7379	0.3832	0.9118	0.9733
	Ag nanoparticles	0.0995	0.9886	3.0004	0.9870	0.7733	0.3443	0.9944
SAM2%	Metronidazole	0.068	0.9127	0.860	0.8082	0.2346	1.296	0.9964
SAA2%	Ag nanoparticles	0.1378	0.9948	4.1551	0.9924	0.7973	0.2716	0.9967
SAA5%	Ag nanoparticles	0.1004	0.9931	3.0239	0.9879	0.6023	0.1338	0.9913

95.10%, 96.46%, 97.01%, and 96.05% for sponges SA1, SA2, SA5, SA6, SA11, SA12, and SAA2%, and SAA5%, respectively, over 48 h.

The values of R^2, n, and K of Ag nanoparticles released from the sponges are summarized in Table 5. The drug release mechanisms of the nanoparticles from the sponges (SA1, SA2, SA5, SA6, SA11, SA12, SA2%, and SAA5%) were best fitted into the Korsmeyer–Peppas model with R^2 ranging between 0.9750 and 0.9992. The n values were 0.5405, 0.5213, and 0.7383 for SA1, SA2, and SA5, respectively, representing a non-Fickian release mechanism (n values greater than 0.5). The n values for SA6, SA11, SA12, SAA2%, and SAA5% were 0.3526, 0.1896, 0.3443, 0.2716, and 0.1338, representing quasi-Fickian diffusion release mechanism (n values less than 0.5).

In vitro cytotoxicity studies

Three sponges (SA1, SAM2%, and SAB2%) were selected for in vitro cytotoxicity studies to illustrate the cell viability of the sponges with either a single drug or a combination of metronidazole with Ag nanoparticles (Fig. 3). The cytotoxicity of the sponge loaded with a combination of metronidazole and Ag nanoparticles (SA1), the sponge loaded with only metronidazole (SAM2%), and the plain sponge (SAB2%) was evaluated by screening these sponges at the concentration of 12.2, 25, 50, and 100 μM of sponges against immortalized human keratinocytes (HaCaT cells). The calculated % cell viability of each sponge against the untreated cells was used to analyze the cytotoxicity results of the sponges. The sponge that retained the

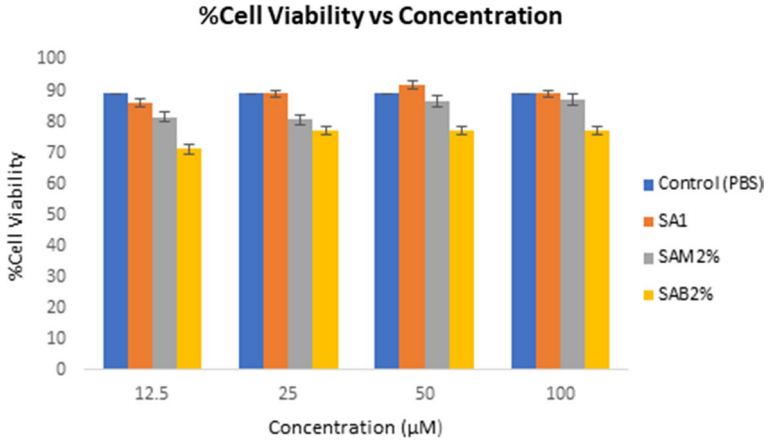

Fig. 3 % Cell viability of sponges at different concentrations (incubated with HaCaT cells for 48 h (p-value = 0.0013 for SA1, p-value = 0.0105 for SAM2% and p-value = 0.0001 for SAB2%)

highest cell viability at the highest concentration (100 μM) was SA1, with a % cell viability of 86.10%, followed by SAM2% with a % cell viability of 81.51%, and SAB2% with a % cell viability of 71.71%. The loading of bioactive agents (metronidazole and Ag nanoparticles) into the sponges revealed a high % cell viability, suggesting that loading the drugs into the wound dressings did not induce any significant cytotoxic effect. All the sponges exhibited good cell viability, indicating non-toxicity and good biocompatibility, which are the ideal features for wound dressing for treating infected wounds.

Zou et al. fabricated gelatin/konjac sponges loaded with gentamicin sulfate and Au nanoparticles for wound healing applications. The in vitro cytotoxicity studies employing MTT assay showed that the cell viability of the murine fibroblast cell line (L929 cells) was more than 80% when incubated with dual drug-incorporated gelatin-based sponges, suggesting good biocompatibility and non-cytotoxicity [37]. These results are similar to the results reported in this study, revealing the non-toxic nature of the wound dressings. Lan et al. demonstrated that gelatin/chitosan sponge-induced cell growth and adhesion of L929 cells, suggesting that these gelatin-based hybrid sponges are biocompatible and non-cytotoxic [74]. Gelatin-based scaffolds have been reported by some researchers to be biocompatible and suitable for biomedical applications without causing toxic side effects. The gelatin/alginate wound dressing materials loaded with silicon carbide nanoparticles reported by Ghanbari et al. demonstrated cell viability that range between 87.9% and 90.3% when incubated with L929 fibroblast cell lines for 72 h, indicating excellent cytocompatibility and non-toxicity [75]. Ghanbari et al. prepared gelatin/alginate scaffolds incorporated with zirconium oxide nanoparticles. The cytotoxicity results showed the capability of these scaffolds to induce cell proliferation and adhesion [76]. Another study by Ghanbari et al. showed that the incorporation of nanoparticles into the gelatin/alginate scaffold-induced significant cell proliferation and viability [77]. Gelatin-alginate scaffolds loaded with carbon nitride quantum dots showed more than 88%

cell viability when cultured with osteosarcoma cell lines, indicating excellent biocompatibility and non-toxicity [78].

In vitro antibacterial analysis

The antibacterial studies were performed to evaluate the antibacterial activity of gelatin/PEG sponges loaded with metronidazole and Ag nanoparticles. The antibacterial efficacy of the sponges against Gram-negative and Gram-positive bacteria strains was observed by comparing their minimum inhibition concentrations (MIC) values to those of the controls (Table 6). The lowest MIC values of the sponges, when compared to the control, were considered to be more effective. The antibacterial activity of the loaded metronidazole in the sponge was retained. The co-loading of metronidazole and Ag nanoparticles into the sponges did not result in improved antibacterial efficacy. All the sponges displayed superior antibacterial efficacy against *Staphylococcus aureus* (SA) except for SA12 than the controls, ampicillin (AMP), streptomycin and nalidixic acid. The antibacterial efficacy of all the sponges was excellent against *Bacillus subtilis* (BS) and *Enterococcus faecalis* (EF) than all the controls employed in the study, except SA6. SA7 and SA10 showed significant antibacterial efficacy against *Staphylococcus epidermidis* (SE) than the controls.

The sponges exhibited good antibacterial efficacy against *Enterobacter cloacae* (ECL) except SA10, SA11, and SA12, than the controls. The antibacterial activity of sponges SA3, SA4, SAA5%, SAM2%, and SAB5% against *Proteus vulgaris* (PV) was excellent when compared to the controls. All the gelatin hybrid sponges showed significant antibacterial activity against *Klebsiella oxytoca* (KO) and *Proteus mirabilis* (PM). SA1, SA5, and SA6 showed MIC values of 31.25 µg/mL against *Pseudomonas aeruginosa* (PA), while SA2, SA3, SA4, SA10, and SA12 MIC value was 15.625 µg/mL, suggesting that they displayed superior antibacterial activity than controls AMP (64 µg/mL), STM (128 µg/mL), and NLD (128 µg/mL). The hybrid sponges SA1, SA2, SA3, SA4, SA8, SA9, SAA2%, SAA5%, and SAM2% displayed good antibacterial efficacy against *Escherichia coli* (EC) with MIC values of 15.625 µg/mL than AMP (26 µg/mL), STM (64 µg/mL), and NLD (512 µg/mL). Sponge SAM2% demonstrated superior antibacterial efficacy against *Klebsiella pneumonia* (KP) with a MIC value of 15.625 µg/mL than AMP, STM, and NLD, with MIC values of 26, 512, and 256 µg/mL, respectively.

Almost all the sponges showed significant and selective antibacterial efficacy against most of the gram-positive bacteria (BS, EF, SE, and SA) and gram-positive bacteria (ECL, KO, PM, PA, and EC) than the controls used. The gelatin/PEG sponges loaded with metronidazole and Ag nanoparticles demonstrated good antibacterial efficacy against the strains of bacteria (*S. epidermidis, P. aeruginosa*, *S. aureus*, *E. coli*, and *P. vulgaris*) that commonly cause wound infections [79, 80], demonstrating that these sponges are potential scaffolds that can be utilized for the management of infected chronic injuries. *P. vulgaris* and *S. epidermidis* are responsible for antibiotic resistance genes, and they can cause biofilms that result in chronic wounds [81]. Biofilms caused by *P. aeruginosa* are generally classified as difficult-to-heal chronic wounds [82]. Metronidazole is effective against resistant strains of

Table 6 Antibacterial results of sponges (MIC values were measured in μg/mL)

	Gram-positive					Gram-negative						
Tested compounds	BS	EF	SE	SA	MS	ECL	PV	KO	PA	PM	EC	KP
SA1	15.625	15.625	500	15.625	500	15.625	500	15.625	31.25	15.625	15.625	500
SA2	15.625	15.625	250	15.625	250	15.625	250	15.625	15.625	15.625	15.625	500
SA3	15.625	15.625	125	15.625	250	15.625	15.625	15.625	15.625	15.625	15.625	500
SA4	15.625	15.625	250	15.625	250	15.625	15.625	15.625	15.625	15.625	15.625	500
SA5	15.625	15.625	500	15.625	500	15.625	500	15.625	31.25	15.625	500	500
SA6	500	500	500	15.625	500	15.625	500	15.625	31.25	15.625	500	500
SA7	15.625	15.625	15.625	15.625	500	15.625	500	15.625	500	15.625	500	500
SA8	15.625	15.625	500	15.625	500	15.625	500	15.625	500	15.625	15.625	500
SA9	15.625	15.625	500	15.625	500	15.625	500	15.625	500	15.625	15.625	500
SA10	15.625	15.625	15.625	15.625	500	250	500	15.625	15.625	15.625	500	500
SA11	15.625	15.625	500	15.625	500	500	500	15.625	500	15.625	500	500
SA12	15.625	15.625	125	31.25	500	250	125	15.625	15.625	15.625	500	500
SAA2%	15.625	15.625	500	15.625	500	15.625	500	15.625	500	15.625	15.625	500
SAA5%	15.625	15.625	500	15.625	500	15.625	15.625	15.625	500	15.625	15.625	500
SAM2%	15.625	15.625	500	15.625	500	15.625	15.625	15.625	500	15.625	15.625	15.625
SAB2%	15.625	15.625	500	15.625	500	15.625	500	15.625	500	15.625	500	500
SAB5%	15.625	15.625	500	15.625	500	15.625	15.625	15.625	500	15.625	500	500
Metronidazole	15.625	15.625	125	15.625	500	125	500	15.625	500	15.625	500	500
Amp	26	26	26	26	26	26	416	26	64	26	26	26
STM	16	128	8	256	4	512	128	16	128	128	64	512
NLD	16	> 512	64	64	512	16	128	8	128	32	512	256

Enterococcus faecalis (ATCC13047) (EF), *Bacillus subtilis* (ATCC19659) (BS), *Mycobacterium smegmatis* (MC2155) (MS), *Escherichia coli* (ATCC25922) (EC), *Enterobacter cloacae* (ATCC13047) (ECL), *Klebsiella pneumonia* (ATCC13882) (KP), *Klebsiella oxytoca* (ATCC8724) (KO), *Proteus vulgaris* (ATCC6380) (PV), *Pseudomonas aeruginosa* (ATCC27853) (PA), *Proteus mirabilis* (ATCC7002) (PM), *Staphylococcus epidermidis* (ATCC14990) (SE), and *Staphylococcus aureus* (ATCC25923) (SA)

P. aeruginosa when utilized in combination therapies [83]. However, it suffers from drug resistance and adverse side effects.

Some research reports have shown that metronidazole-loaded wound dressing scaffolds are effective for the treatment of infected wounds. Brako et al. reported PVP/PCL nanofibers wound dressings loaded with metronidazole. The nanofibers were more effective against *P. aeruginosa* cells than the control, metronidazole creams [84], indicating that the nanofibers are potential wound dressings for the management of bacteria-infected wounds. Metronidazole-loaded gelatin/poly (3-hydroxy butyrate) nanofibrous scaffolds were reported by El-Shanshory et al. with excellent antibacterial activity against *E. aureus* with a diameter of inhibition zone of 5.42 mm [85]. El-Newehy et al. prepared PVA/PEO nanofibers loaded with metronidazole that displayed superior antimicrobial effects against *P. aeruginosa*, *E. coli*, *Penicillium notatum*, *Aspergillus niger*, and *Aspergillus flavus* [86]. Metronidazole-loaded gelatin/PEG-based composite hydrogels prepared by Khade et al. also showed good antibacterial activity against *E. coli* [87]. These preclinical research reports demonstrate that wound dressings loaded with metronidazole are promising systems for treating infected wounds. Many studies have also evaluated the therapeutic efficacy of Ag nanoparticles-loaded materials as potential antibacterial wound dressings.

Ye et al. fabricated gelatin–gelatin sponges cross-linked with tannic acid and incorporated them with Ag nanoparticles. The antimicrobial experiments demonstrated that the addition of Ag nanoparticles improved the antibacterial effects of the sponges against *E. coli* and *S. aureus* [88]. The Ag nanoparticles-loaded gelatin-based sponges reported by Wu et al. showed excellent and sustained antibacterial activity against *Streptococcus mutans* (gram-positive bacteria) with MIC values ranging between 0.5 and 2.1 mm [89]. Other antibacterial studies reported by Rattanaruengsrikul et al. showed that gelatin wound dressings loaded with Ag nanoparticles inhibited 99.7% bacterial growth of *P. aeruginosa*, *S. aureus*, and *E. coli*, common bacterial strains that cause wound infections [90]. Khanha et al. prepared gelatin-based composites loaded with a combination of Ag nanoparticles and curcumin that promoted excellent antibacterial effects against *S. aureus* and *P. aeruginosa* than the composites incorporated with only curcumin [91].

Aktürk et al. synthesized PVA nanofibrous mats incorporated with starch and coated with Ag nanoparticles that exhibited potent growth-inhibitory and excellent antibacterial effects against *S. aureus* and *E. coli* [92]. Kohsari et al. prepared PEO-chitosan antibacterial nanofibrous mats loaded with Ag nanoparticles with more than 99% inhibition effects against *E. coli* and *S. aureus* [93]. Thomas et al. formulated PCL nanofibrous membranes incorporated with Ag nanoparticles with superior antimicrobial activity against *Staphylococcus haemolyticus* and *S. epidermidis* than the pristine membranes [94].

In vitro scratch wound healing assay

In vitro scratch wound-healing assay was performed on sponges SA1 (sponge loaded with metronidazole and Ag nanoparticles) and SAM2% (sponge loaded with Metronidazole only). Both wound dressings displayed high % cell viability.

Wound healing studies were performed at time points of 0, 24, 48, 72, and 96 h to compare the rate of closure of the treated and untreated cells. The wound healing results are shown in Fig. 4a–o. The cells treated with sponge SAM2% exhibited a higher rate of closure than the untreated cells and SA1 treated with HaCaT cells for 96 h as shown in Table 7. SAM2% and SA1 treated with cells exhibited a reduction in the scratch area with a closure rate of 66.68 and 46.61%, respectively, while the untreated cells displayed a closure rate of 29.93% for 96 h (4 days). These results revealed that the sponge loaded with a combination of metronidazole and Ag nanoparticles or loaded with metronidazole alone, significantly accelerated the rate of wound closure in vitro than the untreated scratch cells. SAM2% showed a significant reduction in the scratch area than SA1. Metronidazole loaded in the sponges acts as a chemoattractant to improve cell migration of HaCaT cells, an important feature to restore skin integrity.

Raja and Fathima reported gelatin-based composite wound dressings incorporated with cerium oxide nanoparticles. The in vitro scratch wound healing assay employing scratched NIH-3T3 fibroblast cells that were visualized using a light microscope showed the fastest % reduction in lesion area of $49.4 \pm 0.2\%$ for drug-loaded gelatin composite when compared to the plain gelatin-based composite ($47.3 \pm 0.3\%$) and untreated stretched cells ($44.8 \pm 0.2\%$) for 10 h of the assay [95]. Zhang et al. fabricated gelatin sponges for the treatment of wounds. The in vitro scratch healing analysis showed an accelerated rate of closure of 78% on day 2 of scratch human skin fibroblasts, demonstrating the potential application of gelatin-based sponges in wound healing [96]. Growth factor was loaded to gelatin methacryloyl/poly(3-hydroxybutyrate-co-3-hydroxyvalerate) hybrid patches by Augustine et al. which significantly promoted accelerated wound closure [97].

Conclusion

Gelatin/PEG sponges loaded with metronidazole and Ag nanoparticles were successfully formulated. The porosity of the gelatin-based hybrid sponges was in the range of 15.64–91.10%, and it increased with an increase in the gelatin content used to prepare the sponges, revealing that these sponges can improve cell proliferation and gaseous exchange during wound dressing applications. The in vitro studies (*i.e.*, biodegradability, drug release, cytotoxicity, antibacterial, and scratch wound healing) revealed high % cell viability and promising antibacterial efficacy against Gram-positive bacteria and Gram-negative bacteria, ideal features for wound dressings effective in treating infected wounds. In vitro scratch wound healing studies showed that the cells treated with the sponges promoted cell proliferation, an important feature useful in wound closure than the untreated cells for 96 h, revealing their potential to induce wound healing.

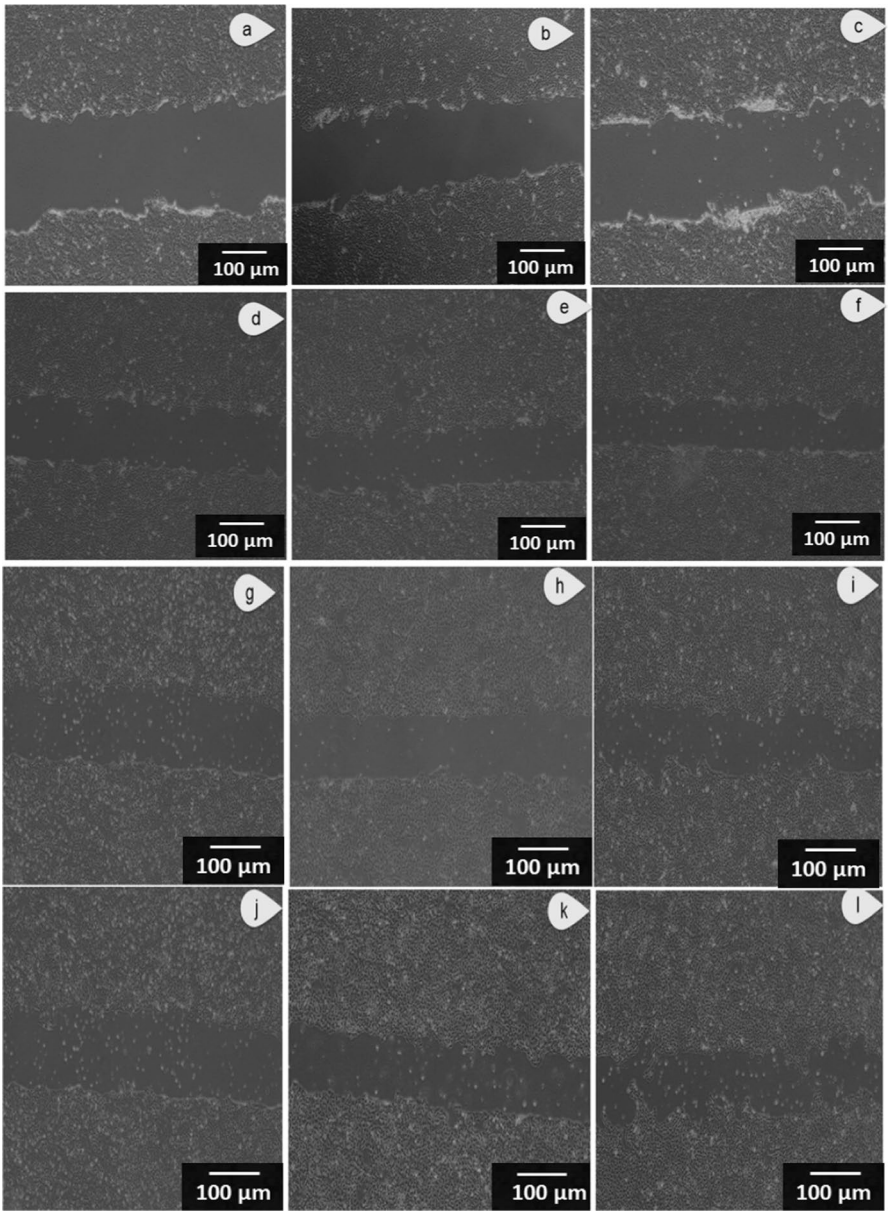

Fig. 4 Wound scratch images **a** Untreated cells at 0 h **b** SA1 at 0 h **c** SAM2% at 0 h **d** untreated cells at 24 h **e** SA1 at 24 h **f** SAM2% at 24 h. Wound scratch images **g** Untreated cells at 48 h **h** SA1 at 48 h **i** SAM2% at 48 h **j** untreated cells at 72 h **k** SA1 at 72 h **l** SAM2% at 72 h. Wound scratch images **m** Untreated cells at 96 h **n** SA1 at 96 h **o** SAM2% at 96 h

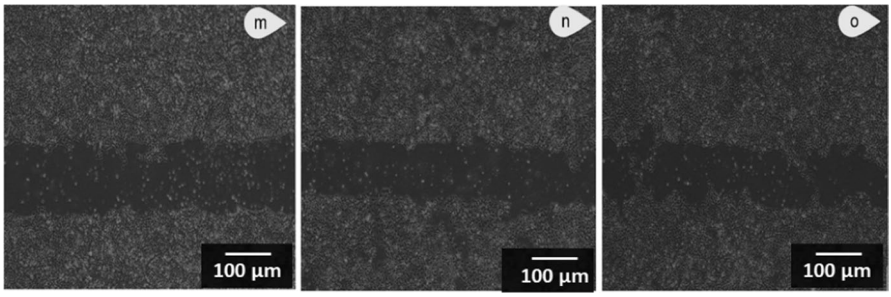

Fig. 4 (continued)

Table 7 Area of the scratch wound for the sponges (0–96 h)

Time (h)	Area (mm^2)		
	Untreated cells	SAM2%	SA1
0	881.032	876.272	823.383
24	758.655	419.124	607.580
48	729.597	311.258	538.212
72	647.623	215.126	481.316
96	617.324	292.061	439.603
Total reduction	263.708 = 29.93%	584.211 = 66.68%	383.78 = 46.61%

(p-value = 0.0037 for SAM2% and 0.0060 for SA1)

Supplementary Information The online version contains supplementary material available at https://doi.org/10.1007/s00289-023-04915-1.

Acknowledgements The financial support of Govan Mbeki Research and Development Centre (GMRDC), University of Fort Hare, South Africa Medical Research Council (SAMRC), and National Research Foundation (NRF), South Africa, toward this research, is hereby acknowledged.

Funding Open access funding provided by University of Fort Hare.

Declarations

Conflict of interest The authors hereby declare no conflict of interest.

References

1. Schreml S, Szeimies RM, Prantl L, Karrer S, Landthaler M, Babilas P (2010) Oxygen in acute and chronic wound healing. Br J Dermatol 163:257–268
2. Debele TA, Su WP (2022) Polysaccharide and protein-based functional wound dressing materials and applications. Int J Polym Mater Polym Biomater 71:87–108
3. Nunan R, Harding KG, Martin P (2014) Clinical challenges of chronic wounds: searching for an optimal animal model to recapitulate their complexity. Dis Model Mech 7:1205–1213
4. Fredric S, Gowda DV, Yashashwini M (2015) Wafers for wound healing. J Chem Pharm Res 7:450–468
5. Davies A, Spickett-Jones F, Jenkins AT, Young AE (2020) A systematic review of intervention studies demonstrates the need to develop a minimum set of indicators to report the presence of burn wound infection. Burns 4:1487–1497
6. Seth AK, Geringer MR, Hong SJ, Leung KP, Mustoe TA, Galiano RD (2012) In vivo modeling of biofilm-infected wounds: a review. J Surg Res 178:330–338
7. Scalise A, Bianchi A, Tartaglione C, Bolletta E, Pierangeli M, Torresetti M, Marazzi M, Di Benedetto G (2015) Microenvironment and microbiology of skin wounds: the role of bacterial biofilms and related factors. Semin Vasc Surg 28:151–159
8. Robson MC (2001) Wound healing; biologic features and approaches to maximize healing trajectories. Curr Problems Surg 38:61–140
9. Chang RY, Morales S, Okamoto Y, Chan HK (2020) Topical application of bacteriophages for treatment of wound in fections. Transl Res 220:153–166
10. Exner M, Bhattacharya S, Christiansen B, Gebel J, Goroncy-Bermes P, Hartemann P, Heeg P, Ilschner C, Kramer A, Larson E, Merkens W (2017) Antibiotic resistance: What is so special about multidrug-resistant gram-negative bacteria? GMS hygiene and infection contr 12:1–24
11. Kirtane AR, Verma M, Karandikar P, Furin J, Langer R, Traverso G (2021) Nanotechnology approaches for global infectious diseases. Nat Nanotech 16:69–84
12. Lv LC, Huang QY, Ding W, Xiao XH, Zhang HY, Xiong LX (2019) Fish gelatin: the novel potential applications. J Funct Foods 63:103581
13. Pati F, Datta P, Adhikari B, Dhara S, Ghosh K, Mohapatra PK (2012) Collagen scaffolds derived from fresh water fish origin and their biocompatibility. J Biomed Mater Res Part A 100:1068–1079
14. Hayashi Y, Yamada S, Guchi KY, Koyama Z, Ikeda T (2012) Chitosan and fish collagen as biomaterials for regenerative medicine. Adv Food Nutr Res 65:107–120
15. Chen SL, Fu RH, Liao SF, Liu SP, Lin SZ, Wang YC (2018) A PEG-based hydrogel for effective wound care management. Cell Transplant 27:275–284
16. Kardan T, Mohammadi R, Taghavifar S, Cheraghi M, Yahoo A, Mohammadnejad K (2021) Polyethylene glycol-based nanocerium improves healing responses in excisional and incisional wound models in rats. Inter J Low Extrem Wounds 20:263–271
17. Yang Y, Xia T, Chen F, Wei W, Liu C, He S, Li X (2012) Electrospun fibers with plasmid bFGF polyplex loadings promote skin wound healing in diabetic rats. Mol Pharm 9:48–58
18. Yang X, Liu W, Xi G, Wang M, Liang B, Shi Y, Feng Y, Ren X, Shi C (2019) Fabricating antimicrobial peptide-immobilized starch sponges for hemorrhage control and antibacterial treatment. Carbohydr Polym 222:115012
19. Feng Y, Li X, Zhang Q, Yan S, Guo Y, Li M, You R (2019) Mechanically robust and flexible silk protein/polysaccharide composite sponges for wound dressing. Carbohydr Polym 216:17–24
20. Villamizar-Sarmiento MG, Moreno-Villoslada I, Martínez S, Giacaman A, Miranda V, Vidal A, Orellana SL, Concha M, Pavicic F, Lisoni JG, Leyton L (2019) Ionic nanocomplexes of hyaluronic acid and polyarginine to form solid materials: a green methodology to obtain sponges with biomedical potential. Nanomaterials 9:944
21. Ma R, Wang Y, Qi H, Shi C, Wei G, Xiao L, Huang Z, Liu S, Yu H, Teng C, Liu H (2019) Nanocomposite sponges of sodium alginate/graphene oxide/polyvinyl alcohol as potential wound dressing: in vitro and in vivo evaluation. Compos Part B Eng 167:396–405
22. Yang G, Xiao Z, Long H, Ma K, Zhang J, Ren X, Zhang J (2018) Assessment of the characteristics and biocompatibility of gelatin sponge scaffolds prepared by various crosslinking methods. Sci Rep 8:1–3
23. Ulubayram K, Aksu E, Gurhan SI, Serbetci K, Hasirci N (2002) Cytotoxicity evaluation of gelatin sponges prepared with different cross-linking agents. J Biomat Scie Poly Ed 13:1203–1219

24. Kabiri M, Emami SH, Rafinia M, Tahriri M (2011) Preparation and characterization of absorbable hemostat crosslinked gelatin sponges for surgical applications. Curr App Phy 1:457–461
25. Lu B, Wang T, Li Z, Dai F, Lv L, Tang F, Yu K, Liu J, Lan G (2016) Healing of skin wounds with a chitosan–gelatin sponge loaded with tannins and platelet-rich plasma. Int J Biol Macromol 82:884–891
26. Abo-Shama UH, El-Gendy H, Mousa WS, Hamouda RA, Yousuf WE, Hetta HF, Abdeen EE (2020) Synergistic and antagonistic effects of metal nanoparticles in combination with antibiotics against some reference strains of pathogenic microorganisms. Infe Drug Res 13:351–362
27. Dingsdag SA, Hunter N (2018) Metronidazole: an update on metabolism, structure–cytotoxicity and resistance mechanisms. J Antimicrob Chemother 73:265–279
28. Kurian M, Ganapathy D, Jain AR (2018) Recent advances of metronidazole-a review. Drug Invent Today 10:3536
29. Ousey K (2018) The role of topical metronidazole in the management of infected wounds. Wounds UK 14:105–109
30. Castro DL, Santos VL (2015) Controlling wound odor with metronidazole: a systematic review. Rev Esc Enferm USP 49:0858–0863
31. Karami M, Ghanbari M, Alshamsi HA, Rashki S, Salavati-Niasari M (2021) Facile fabrication of Tl_4HgI_6 nanostructures as novel antibacterial and antibiofilm agents and photocatalysts in the degradation of organic pollutants. Inorg Chem Front 8:2442–2460
32. Ghanbari M, Salavati-Niasari M (2021) Copper iodide decorated graphitic carbon nitride sheets with enhanced visible-light response for photocatalytic organic pollutant removal and antibacterial activities. Ecotoxic Environ Saf 8:2442–2460
33. Gupta A, Briffa SM, Swingler S, Gibson H, Kannappan V, Adamus G, Kowalczuk M, Martin C, Radecka I (2020) Synthesis of silver nanoparticles using curcumin-cyclodextrins loaded into bacterial cellulose-based hydrogels for wound dressing applications. Biomacromol 21:1802–1811
34. Das CA, Kumar VG, Dhas TS, Karthick V, Govindaraju K, Joselin JM, Baalamurugan J (2020) Antibacterial activity of silver nanoparticles (biosynthesis): a short review on recent advances. Biocatal Agric Biotechnol 27:101593
35. Konop M, Damps T, Misicka A, Rudnicka L (2016) Certain aspects of silver and silver nanoparticles in wound care: a minireview. J Nanomater 2016:1–10
36. Silva MM, Aguiar MI, Rodrigues AB, Miranda MD, Araújo MÂ, Rolim IL (2017) The use of nanoparticles in wound treatment: a systematic review. Rev Escola Enferm USP 51:e0327
37. Zou Y, Xie R, Hu E, Qian P, Lu B, Lan G, Lu F (2020) Protein-reduced gold nanoparticles mixed with gentamicin sulfate and loaded into konjac/gelatin sponge heal wounds and kill drug-resistant bacteria. Int J Biol Macromol 148:921–931
38. Wang X, Guo J, Zhang Q, Zhu S, Liu L, Jiang X, Wei DH, Liu RS, Li L (2020) Gelatin sponge functionalized with gold/silver clusters for antibacterial application. Nanotechnology 31:134004
39. Jaiswal A, Sanpui P, Chattopadhyay A, Ghosh SS (2011) Investigating fluorescence quenching of ZnS quantum dots by silver nanoparticles. Plasmonics 6:125–132
40. Nerkar D, Rajwade M, Jaware S, Jog M (2020) Synthesis and characterization of polyvinyl alcohopolypyrrole-silver nanocomposite polymer films. Int J Nano Dimens 11:205–214
41. Neto AD, dos Santos Cruz CF, Serafini MR, dos Passos MP, de Carvalho YM, Matos CR, Nunes PS (2017) Usnic acid-incorporated alginate and gelatin sponges prepared by freeze-drying for biomedical applications. J Therm Anal Calorim 127:1707–1714
42. Wen Y, Yu B, Zhu Z, Yang Z, Shao W (2020) Synthesis of antibacterial gelatin/sodium alginate sponges and their antibacterial activity. Polymers 12:1926
43. Naghshineh N, Tahvildari K, Nozari M (2019) Preparation of chitosan, sodium alginate, gelatin and collagen biodegradable sponge composites and their application in wound healing and curcumin delivery. J Polym Environ 27:2819–2830
44. Xie Y, Yi ZX, Wang JX, Hou TG, Jiang Q (2018) Carboxymethyl konjac glucomannan-crosslinked chitosan sponges for wound dressing. Int J Biol Macromol 112:1225–1233
45. Arif MM, Fauzi MB, Nordin A, Hiraoka Y, Tabata Y, Yunus MH (2020) Fabrication of bio-based gelatin sponge for potential use as a functional acellular skin substitute. Polymers 12:2678
46. Tawfeek HM, Abou-Taleb DA, Badary DM, Ibrahim M, Abdellatif AA (2020) Pharmaceutical, clinical, and immunohistochemical studies of metformin hydrochloride topical hydrogel for wound healing application. Arch Dermatol Res 312:113–121

47. Fonkui TY, Ikhile MI, Muganza FM, Fotsing MC, Arderne C, Siwe-Noundou X, Krause RW, Ndinteh DT, Njobeh PB (2018) Synthesis, characterization and biological applications of novel Schiff bases of 2-(trifluoromethoxy) aniline. J Chin Pharm Sci 27:307–323
48. Felice F, Zambito Y, Belardinelli E, Fabiano A, Santoni T, Di Stefano R (2015) Effect of different chitosan derivatives on in vitro scratch wound assay: a comparative study. Int J Biol Macromol 76:236–241
49. Suarez-Arnedo A, Figueroa FT, Clavijo C, Arbeláez P, Cruz JC, Muñoz-Camargo C (2020) An image J plugin for the high throughput image analysis of in vitro scratch wound healing assays. PLoS ONE 15:e0232565
50. Cheng Y, Hu Z, Zhao Y, Zou Z, Lu S, Zhang B, Li S (2019) Sponges of carboxymethyl chitosan grafted with collagen peptides for wound healing. Int J Mol Sci 20:3890
51. Ranzato E, Patrone M, Mazzucco L, Burlando B (2008) Platelet lysate stimulates wound repair of HaCaT keratinocytes. Br J Dermatol 159:537–545
52. Alim-Al-Razy M, Bayazid GA, Rahman RU, Bosu R, Shamma SS (2020) Silver nanoparticle synthesis, UV-vis spectroscopy to find particle size and measure resistance of colloidal solution. J Phys Confr Ser 1706:012020
53. Singh S, Bharti A, Meena VK (2015) Green synthesis of multi-shaped silver nanoparticles: optical, morphological and antibacterial properties. J Mater Sci Mater Electron 26:3638–3648
54. Anandalakshmi K, Venugobal J, Ramasamy V (2016) Characterization of silver nanoparticles by green synthesis method using *Pedalium murex* leaf extract and their antibacterial activity. Appl Nanosci 6:399–408
55. Li D, Ye Y, Li D, Li X, Mu C (2016) Biological properties of dialdehyde carboxymethyl cellulose crosslinked gelatin–PEG composite hydrogel fibers for wound dressings. Carbohydr Polym 137:508–514
56. Kim SE, Heo DN, Lee JB, Kim JR, Park SH, Jeon SH, Kwon IK (2009) Electrospun gelatin/polyurethane blended nanofibers for wound healing. Biomed Mater 4:044106
57. Chen Y, Lu W, Guo Y, Zhu Y, Song Y (2019) Electrospun gelatin fibers surface loaded ZnO particles as a potential biodegradable antibacterial wound dressing. Nanomaterials 9:525
58. Fan L, Yang H, Yang J, Peng M, Hu J (2016) Preparation and characterization of chitosan/gelatin/PVA hydrogel for wound dressings. Carbohydr Polym 146:427–434
59. Trivedi MK, Patil S, Shettigar H, Bairwa K, Jana S (2015) Spectroscopic characterization of biofield treated metronidazole and tinidazole. Med Chem 5:340–344
60. Arif D, Niazi MB, Ul-Haq N, Anwar MN, Hashmi E (2015) Preparation of antibacterial cotton fabric using chitosan-silver nanoparticles. Fibers Polym 16:1519–1526
61. Gharibshahi L, Saion E, Gharibshahi E, Shaari AH, Matori KA (2017) Structural and optical properties of Ag nanoparticles synthesized by thermal treatment method. Materials (Basel) 10:402
62. Wang B, Johnson A, Li W (2020) Development of an extracellular matrix- enriched gelatin sponge for liver wound dressing. J Biomed Mater Res A 108:2057–2068
63. Ulubayram K, Cakar AN, Korkusuz P, Ertan C, Hasirci N (2001) EGF containing gelatin-based wound dressings. Biomaterials 22:1345–1356
64. Hajosch R, Suckfuell M, Oesser S, Ahlers M, Flechsenhar K, Schlosshauer B (2010) A novel gelatin sponge for accelerated hemostasis. J Biomed Mater Res B Appl Biomater 94:372–379
65. Imani R, Rafienia M, Hojjati Emami S (2013) Synthesis and characterization of glutaraldehyde-based crosslinked gelatin as a local hemostat sponge in surgery: an in vitro study. Biomed Mater Eng 23:211–224
66. Choi SM, Singh D, Kumar A, Oh TH, Cho YW, Han SS (2013) Porous three-dimensional PVA/gelatin sponge for skin tissue engineering. Int J Polym Mater Polym Biomater 62:384–389
67. Ngece K, Aderibigbe BA, Ndinteh DT, Fonkui YT, Kumar P (2021) Alginate-gum acacia based sponges as potential wound dressings for exuding and bleeding wounds. Int J Biol Macromol 172:350–359
68. Ndlovu SP, Ngece K, Alven S, Aderibigbe BA (2021) Gelatin-based hybrid scaffolds: promising wound dressings. Polymers 13:2959
69. El Fawal G, Hong H, Mo X, Wang H (2021) Fabrication of scaffold based on gelatin and polycaprolactone (PCL) for wound dressing application. J Drug Deliv Sci Technol 63:102501
70. Sakthiguru N, Sithique MA (2020) Fabrication of bioinspired chitosan/gelatin/allantoin biocomposite film for wound dressing application. Int J Biol Macromol 152:873–883

71. Mbese Z, Alven S, Aderibigbe BA (2021) Collagen-based nanofibers for skin regeneration and wound dressing applications. Polymers 13:4368
72. Huang X, Brazel CS (2001) On the importance and mechanisms of burst release in matrix-controlled drug delivery systems. J Control Release 73:121–136
73. Ye S, Jiang L, Su C, Zhu Z, Wen Y, Shao W (2019) Development of gelatin/bacterial cellulose-composite sponges as potential natural wound dressings. Int J Biol Macromol 133:148–155
74. Lan G, Lu B, Wang T, Wang L, Chen J, Yu K, Liu J, Dai F, Wu D (2015) Chitosan/gelatin composite sponge is an absorbable surgical hemostatic agent. Colloids Surf B Biointerfaces 136:1026–1034
75. Ghanbari M, Salavati-Niasari M, Mohandes F, Firouzi Z (2022) Modified silicon carbide NPs reinforced nanocomposite hydrogels based on alginate-gelatin by with high mechanical properties for tissue engineering. Arabian J Chem 15:103520
76. Ghanbari M, Salavati-Niasari M, Mohandes F, Firouzi Z, Mousavi S-D (2021) The impact of zirconium oxide nanoparticles content on alginate dialdehyde-gelatin scaffolds in cartilage tissue engineering. J Mol Liquids 335:116531
77. Ghanbari M, Salavati-Niasari M, Mohandes F, Dolatyar B, Zeynali B (2021) In vitro study of alginate–gelatin scaffolds incorporated with silica NPs as injectable, biodegradable hydrogels. RSC Adv 11:16688
78. Ghanbari M, Salavati-Niasari M, Mohandes F (2021) Injectable hydrogels based on oxidized alginate-gelatin reinforced by carbon nitride quantum dots for tissue engineering. Inter J Pharm 602:120660
79. Alwan MJ, Lafta IJ, Hamzah AM (2011) Bacterial isolation from burn wound infections and studying ا لة مج ة كوف ال لوم لع ل ية ب ط ال يطري ب ال (Kufa J Vet Med Sci 2:1.
80. Almeida GC, dos Santos MM, Lima NG, Cidral TA, Melo MC, Lima KC (2014) Prevalence and factors associated with wound colonization by *Staphylococcus spp*. and *Staphylococcus aureus* in hospitalized patients in inland northeastern Brazil: a cross-sectional study. BMC Infect Dis 14:1–8
81. Kwiecinska-Pirog J, Skowron K, Bartczak W, Gospodarek-Komkowska E (2016) The ciprofloxacin impact on biofilm formation by *Proteus mirabilis* and *P vulgaris* strains. Jundishapur journal of microbiology 9(4):e32656
82. Bjarnsholt T, Kirketerp- Møller K, Jensen PØ, Madsen KG, Phipps R, Krogfelt K, Høiby N, Givskov M (2008) Why chronic wounds will not heal: a novel hypothesis. Wound Repair Regen 16:2–10
83. Miller B, Popejoy MW, Hershberger E, Steenbergen JN, Alverdy J (2016) Characteristics and outcomes of complicated intra-abdominal infections involving *Pseudomonas aeruginosa* from a randomized, double-blind, phase 3 ceftolozane-tazobactam study. Antimicrob Agents Chemother 60:4387–4390
84. Brako F, Luo C, Matharu RK, Ciric L, Harker A, Edirisinghe M, Craig DQ (2020) A portable device for the generation of drug-loaded three-compartmental fibers containing metronidazole and iodine for topical application. Pharmaceutics 12:373
85. El-Shanshory AA, Agwa MM, Abd-Elhamid AI, Soliman HM, Mo X, Kenawy ER (2022) Metronidazole topically immobilized electrospun nanofibrous scaffold: novel secondary intention wound healing accelerator. Polymers 14:454
86. El-Newehy MH, Al-Deyab SS, Kenawy ER, Abdel-Megeed A (2012) Fabrication of electrospun-antimicrobial nanofibers containing metronidazole using nanospider technology. Fibers Polym 13:709–717
87. Khade SM, Behera B, Sagiri SS, Singh VK, Thirugnanam A, Pal K, Ray SS, Pradhan DK, Bhattacharya MK (2014) Gelatin–PEG based metronidazole-loaded vaginal delivery systems: preparation, characterization and in vitro antimicrobial efficiency. Iran Polym J 23:171–184
88. Ye H, Cheng J, Yu K (2019) In situ reduction of silver nanoparticles by gelatin to obtain porous silver nanoparticle/chitosan composites with enhanced antimicrobial and wound-healing activity. Int J Biol Macromol 121:633–642
89. Wu L, Gareiss SK, Morrow BR, Babu JP, Hottel T, Garcia-Godoy F, Li F, Hong L (2019) Antibacterial properties of silver-loaded gelatin sponges prepared with silver diamine fluoride. Am J Dent 32:276–280
90. Rattanaruengsrikul V, Pimpha N, Supaphol P (2012) In vitro efficacy and toxicology evaluation of silver nanoparticle- loaded gelatin hydrogel pads as antibacterial wound dressings. J Appl Polym Sci 124:1668–1682

91. Khanh LL, Truc NT, Dat NT, Nghi NT, Van Toi V, Hoai NT, Quyen TN, Loan TT, Hiep NT (2019) Gelatin-stabilized composites of silver nanoparticles and curcumin: characterization, antibacterial and antioxidant study. Sci Technol Adv Mater 20:276
92. Aktürk A, Taygun ME, Güler FK, Goller G, Küçükbayrak S (2019) Fabrication of antibacterial polyvinylalcohol nanocomposite mats with soluble starch coated silver nanoparticles. Colloids Surf A Physicochem Eng Aspects 562:255–262
93. Kohsari I, Shariatinia Z, Pourmortazavi SM (2016) Antibacterial electrospun chitosan–polyethylene oxide nanocomposite mats containing bioactive silver nanoparticles. Carbohydr Polym 140:287–298
94. Thomas R, Soumya KR, Mathew J, Radhakrishnan EK (2015) Electrospun polycaprolactone membrane incorporated with biosynthesized silver nanoparticles as effective wound dressing material. Appl Biochem Biotechnol 176:2213–2224
95. Raja IS, Fathima NN (2018) Gelatin–cerium oxide nanocomposite for enhanced excisional wound healing. ACS Appl Bio Mater 1:487–495
96. Zhang H, Liu S, Yang X, Chen N, Pang F, Chen Z, Wang T, Zhou J, Ren F, Xu X, Li T (2018) LED phototherapy with gelatin sponge promotes wound healing in mice. Photochem Photobiol 94:179–185
97. Augustine R, Hasan A, Dalvi YB, Rehman SR, Varghese R, Unni RN, Yalcin HC, Alfkey R, Thomas S, Al Moustafa AE (2021) Growth factor loaded in situ photocrosslinkable poly (3-hydroxybutyrate-co-3-hydroxyvalerate)/gelatin methacryloyl hybrid patch for diabetic wound healing. Mater Sci Eng C 118:111519

Authors and Affiliations

Sibusiso Alven[1] · S. A. Adeyemi[2] · P. Ubanako[2] · D. T. Ndinteh[3] · Y. E. Choonara[2] · B. A. Aderibigbe[1]

✉ B. A. Aderibigbe
blessingaderibigbe@gmail.com

[1] Department of Chemistry, University of Fort Hare, Alice Campus, Alice, Eastern Cape, South Africa

[2] Wits Advanced Drug Delivery Platform Research Unit, Department of Pharmacy and Pharmacology, Faculty of Health Sciences, School of Therapeutic Science, University of the Witwatersrand, Johannesburg, South Africa

[3] Drug Discovery and Smart Molecules Research labs, Centre for Natural Product Research, Department of Chemical Sciences, University of Johannesburg, Doornfontein Campus, Johannesburg, South Africa